

Article

MHD Mixed Convection in a Lid-Driven Cavity with a Bottom Trapezoidal Body: Two-Phase Nanofluid Model

Muhammad Adil Sadiq ¹, Ammar I. Alsabery ^{2,3}  and Ishak Hashim ^{3,*}¹ Department of Mathematics, DCC-KFUPM Box 5084, Dhahran 31261, Saudi Arabia; adilsadiq@kfupm.edu.sa² Refrigeration & Air-conditioning Technical Engineering Department, College of Technical Engineering, The Islamic University, Najaf 54001, Iraq; ammar_e_2011@yahoo.com or alsabery_a@ukm.edu.my³ School of Mathematical Sciences, Faculty of Science & Technology, Universiti Kebangsaan Malaysia, Bangi 43600, Selangor, Malaysia

* Correspondence: ishak_h@ukm.edu.my; Tel.: +603-8921-5758

Received: 6 October 2018; Accepted: 23 October 2018; Published: 28 October 2018



Abstract: The current work examines the effects of a bottom trapezoidal solid body and a magnetic field on mixed convection in a lid-driven square cavity. The Al_2O_3 -water nanofluid used is assumed to obey Buongiorno's two-phase model. An isothermal heater is placed on the bottom base of the trapezoid solid body, while the cavity's vertical walls are kept cold at temperature T_c . The top moving wall and the remaining portions of the cavity's bottom wall are thermally insulated. The Galerkin weighted residual finite element method is employed to solve the dimensionless governing equations. The parameters of interest are the Richardson number ($0.01 \leq Ri \leq 100$), Hartmann number ($0 \leq Ha \leq 50$), nanoparticle volume fraction ($0 \leq \phi \leq 0.04$), and the length of the bottom base of the trapezoidal solid body. The obtained results show that increasing the Richardson number or decreasing the Hartmann number tends to increase the heat transfer rate. In addition, both the thermophoresis and Brownian motion greatly improve the convection heat transfer. It is believed that the current work is a good contribution to many engineering applications such as building design, thermal management of solar energy systems, electronics and heat exchange.

Keywords: Brownian motion; lid-driven cavity; magnetic field; solid trapezoidal body; thermophoresis; two-phase nanofluid model

1. Introduction

Mixed convection mechanism is important for controlling heat transfer in many applications, such as electronic systems and nuclear reactors. Mixed convection in cavities can be easily realised by moving surfaces [1]. Lid-driven cavities appear in many engineering applications, such as oil extraction, design of heat exchangers, crystal growth and float glass production, and cooling of electronic equipment [2]. Reference Torrance et al. [3] considered the effects of an upper moving wall on convection in a rectangular cavity. Moallemi and Jang [4] considered the effects of the Prandtl number on mixed convection in a lid-driven square cavity. They found that the temperature distribution and the flow field are clearly influenced by the Prandtl number. The steady mixed convection heat transfer problem in a double lid-driven square cavity was investigated numerically using the finite control volume by Oztop and Dagtekin [5]. Reference Al-Amiri et al. [6] employed the Galerkin weighted residual method to study steady mixed convection in a lid-driven square cavity. Reference Sharif [7] studied laminar mixed convection in an inclined lid-driven cavity. The steady mixed convection in a water-filled square lid-driven cavity in the presence of partial slip condition was

investigated by Ismael et al. [8] who showed that the heat transfer rate increases with the Richardson number. Reference Ismael [9] considered mixed convection in a cavity with an arc-shaped moving wall.

The use of nanofluids could help to enhance heat transfer and the process of heat removal. Nanofluids are defined as the addition of nanoparticles (<100 nm-diameter), like metal or ceramics, to base fluids that have a very low thermal conductivity, like water and oil. The problem of mixed convection in a double lid-driven square cavity filled with Cu-water nanofluid was reported by Tiwari and Das [10]. The flow and heat transfer were shown to be affected by the Richardson number, the solid volume fraction, and the moving walls' directions. There are two models for nanofluids: the single-phase (homogenous) and two-phase models. In the single-phase model, both the nanoparticles and fluid phase are assumed to be in thermal equilibrium, i.e., the fluid-nanoparticles' slip velocity is negligible [1]. Many studies have considered the effects of the single-phase nanofluid model on mixed convective heat transfer inside a lid-driven cavity. Reference Talebi et al. [11] numerically investigated the mixed convection of nanofluids in a lid-driven square cavity. They observed that increasing the Reynolds number tended to reduce the effects of the solid volume fraction. Reference Chamkha and Abu-Nada [12] studied the effects of two different viscosity models on the steady mixed convection of Al₂O₃-water nanofluid in a double lid-driven cavity. Reference Karimipour et al. [13] considered the mixed convection of Cu-water nanofluid in an inclined lid-driven cavity using the lattice Boltzmann method. They found that increasing the nanoparticle volume fraction had the effect of increasing the average Nusselt number. The unsteady natural convection in a nanofluid-filled trapezoidal cavity with a non-uniform side-wall temperature was studied by Alsabery et al. [14].

The slip velocity between the base fluid and nanoparticles was shown experimentally to be non-negligible by Wen and Ding [15]. Thermophoresis and Brownian diffusion are the two main nanofluid slip mechanisms of the two-phase nanofluid model of Buongiorno [16]. A number of investigators have employed the two-phase nanofluid model to model and discuss nanofluid heat transfer. Considering the two-phase model, Alinia et al. [17] numerically studied the mixed convection of a nanofluid in an inclined double lid-driven square cavity. Adding the SiO₂ nanoparticles was shown to greatly enhance the convection heat transfer. Using the control volume based finite element method, Sheikholeslami et al. [18] studied convection heat transfer inside a semi-annulus enclosure based on the two-phase nanofluid model. They observed that the Nusselt number decreased with the Lewis number. Reference Sheremet and Pop [19] reported the problem of the steady laminar mixed convection and heat transfer of a nanofluid in a lid-driven square cavity. The mixed convection of alumina-water nanofluid in microchannels was investigated by Malvandi and Ganji [20] using a modified two-phase model of Buongiorno. Garoosi and Talebi [21] studied the effects of the two-phase model on the conjugate natural and mixed convection of a nanofluid in a square cavity. Recently, Alsabery et al. [22] examined the effects of a solid inner insert on the mixed convection of a two-phase nanofluid model in a double lid-driven square cavity. They observed various effects on the rate of heat transfer with the augmentation of nanoparticles at a low Reynolds number and high Richardson number.

Recently, more emphasis has been placed on studying the effect of a magnetic field on the convection heat transfer in cavities [23,24]. Reference Chamkha [25] investigated the effects of magnetic field and internal heat generation on mixed convection in a lid-driven cavity. The results showed that the magnetic field reduced the average Nusselt number. MHD mixed convection and heat transfer in a lid-driven square cavity with a corner heater was reported by Öztop et al. [26]. They found that increasing the Hartmann number reduced the heat transfer. Reference Chatterjee [27] investigated the effect of a heat source on MHD mixed convection in a lid-driven square cavity. Reference Selimefendigil et al. [28] studied the effect of an inclined magnetic field on MHD mixed convection and entropy generation in a nanofluid-filled lid-driven cavity. MHD mixed convection of a nanofluid in a partially-heated wavy-walled lid-driven cavity was considered by Öztop et al. [29]. They found that the Hartmann and Richardson

numbers affected the heat transfer rate with the augmentation of the nanoparticle volume fraction. Reference Chamkha et al. [30] considered the effects of a heat source/sink and a partial slip condition on the MHD mixed convection and entropy generation of Cu–water nanofluid in a lid-driven porous cavity. Recently, the MHD mixed convection of a two-phase nanofluid model in a lid-driven square cavity with an inner solid block and corner heater was studied by Alsabery et al. [31]. They observed that increasing the concentration of the nanoparticles by more than 2% had negative effects on the rate of heat transfer.

To the best of the authors' knowledge, no study has been conducted on the MHD mixed convection of a nanofluid in a lid-driven cavity with a bottom trapezoidal body. We employ the two-phase nanofluid model of Buongiorno and the cavity is heated from below at the bottom base of the trapezoidal body. It is believed that the current work is a good contribution to many engineering applications such as building design, thermal management of solar energy systems, electronics, and heat exchange.

2. Mathematical Formulation

Consider a lid-driven square cavity of length L filled with a water-based nanofluid with Al_2O_3 nanoparticles. The cavity contains a bottom trapezoidal body with a bottom base of length h , a top base of length $h/2$, and height d , as shown in Figure 1.

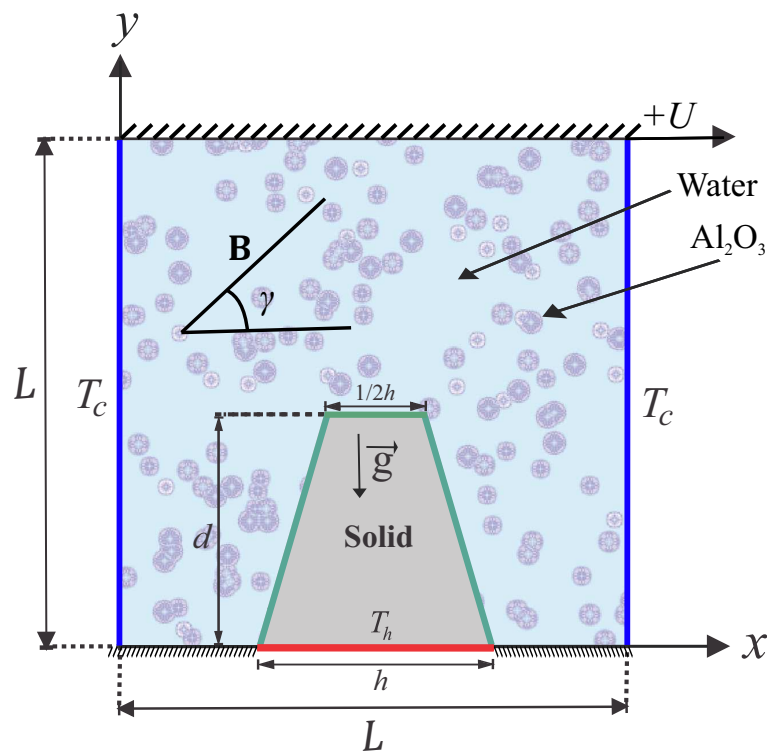


Figure 1. Sketch of the problem geometry.

The bottom base of the trapezoidal body is heated at a higher temperature, T_h . Both the left and right walls are kept at a cold temperature, T_c , while the top moving wall and the remaining parts of the bottom wall are thermally insulated. The acceleration due to gravity is assumed to be vertically downward. The applied magnetic field is uniform and inclined at angle γ . All four boundaries are taken to be impermeable. The fluid physical properties are considered to be constant except for the density (Boussinesq approximation). The flow is steady and laminar. The governing equations are as follows:

$$\nabla \cdot \mathbf{v} = 0, \quad (1)$$

$$\rho_{nf} \mathbf{v} \cdot \nabla \mathbf{v} = -\nabla p + \nabla \cdot (\mu_{nf} \nabla \mathbf{v}) + (\rho\beta)_{nf} (T - T_c) \vec{g} + \sigma_{nf} \mathbf{v} \times \vec{\mathbf{B}}, \quad (2)$$

$$(\rho C_p)_{nf} \mathbf{v} \cdot \nabla T_{nf} = -\nabla \cdot (k_{nf} \nabla T_{nf}) - C_{p,p} J_p \cdot \nabla T_{nf}, \quad (3)$$

$$\mathbf{v} \cdot \nabla \varphi = -\frac{1}{\rho_p} \nabla \cdot J_p, \quad (4)$$

where \mathbf{v} is the velocity vector, p is the pressure, T is the temperature, $\vec{\mathbf{B}}$ is the magnetic field, \vec{g} is the gravitational acceleration vector, and φ and J_p are, respectively, the local volume fraction of nanoparticles and the nanoparticles' mass flux. The trapezoidal body's energy equation is

$$\nabla T_w = 0. \quad (5)$$

The nanoparticles' mass flux J_p can be written as (Buongiorno's model):

$$J_p = J_{p,B} + J_{p,T}, \quad (6)$$

where

$$J_{p,B} = -\rho_p D_B \nabla \varphi, \quad D_B = \frac{k_b T}{3\pi \mu_f d_p}, \quad (7)$$

$$J_{p,T} = -\rho_p D_T \nabla T, \quad D_T = 0.26 \frac{k_f}{2k_f + k_p} \frac{\mu_f}{\rho_f T} \varphi. \quad (8)$$

The nanofluid's heat capacitance, effective thermal diffusivity, effective density, and thermal expansion coefficient are given as, respectively,

$$(\rho C_p)_{nf} = (1 - \varphi)(\rho C_p)_f + \varphi(\rho C_p)_p, \quad (9)$$

$$\alpha_{nf} = \frac{k_{nf}}{(\rho C_p)_{nf}}, \quad (10)$$

$$\rho_{nf} = (1 - \varphi)\rho_f + \varphi\rho_p, \quad (11)$$

$$(\rho\beta)_{nf} = (1 - \varphi)(\rho\beta)_f + \varphi(\rho\beta)_p. \quad (12)$$

The electrical conductivity, dynamic viscosity and thermal conductivity ratios of Al₂O₃-water nanofluid (33 nm particle-size in the ambient condition) are, respectively (cf. [32,33]),

$$\frac{\sigma_{nf}}{\sigma_f} = 1 + \frac{3 \left(\frac{\sigma_p}{\sigma_f} - 1 \right) \varphi}{\left(\frac{\sigma_p}{\sigma_f} + 2 \right) - \left(\frac{\sigma_p}{\sigma_f} - 1 \right) \varphi}, \quad (13)$$

$$\frac{\mu_{nf}}{\mu_f} = \frac{1}{1 - 34.87 \left(d_p/d_f \right)^{-0.3} \varphi^{1.03}}, \quad (14)$$

$$\frac{k_{nf}}{k_f} = 1 + 4.4 \text{Re}_B^{0.4} \text{Pr}^{0.66} \left(\frac{T}{T_{fr}} \right)^{10} \left(\frac{k_p}{k_f} \right)^{0.03} \varphi^{0.66}, \quad (15)$$

where $\text{Re}_B = \rho_f u_B d_p / \mu_f$. Here, $u_B = 2k_b T / \pi \mu_f d_p^2$ with $k_b = 1.380648 \times 10^{-23}$ (J/K) is the Boltzmann constant, and $l_f = 0.17$ nm is the mean path of the fluid particles. The water molecular diameter [33] is

$$d_f = 6M/N\pi\rho_f = \left(\frac{6 \times 0.01801528}{6.022 \times 10^{23} \times \pi \times 998.26} \right)^{1/3} = 3.85 \times 10^{-10} \text{ m}, \quad (16)$$

where M , N and ρ_f are, respectively, the molecular weight of water, the Avogadro number, and the density of the base fluid at standard temperature (310 K).

The governing equations can be made dimensionless if we take the following non-dimensional variables

$$X = \frac{x}{L}, Y = \frac{y}{L}, \mathbf{V} = \frac{\mathbf{v}}{U_0}, P = \frac{pL^2}{\rho_{nf}v_f^2}, \varphi^* = \frac{\varphi}{\phi}, D_B^* = \frac{D_B}{D_{B0}}, D_T^* = \frac{D_T}{D_{T0}},$$

$$\delta = \frac{T_c}{T_h - T_c}, \theta_{nf} = \frac{T_{nf} - T_c}{T_h - T_c}, \theta_w = \frac{T_w - T_c}{T_h - T_c}, D = \frac{d}{L}, H = \frac{h}{L}.$$

Hence, the dimensionless governing equations are

$$\nabla \cdot \mathbf{V} = 0, \quad (17)$$

$$\mathbf{V} \cdot \nabla \mathbf{V} = -\nabla P + \frac{\rho_f \mu_{nf}}{\rho_{nf} \mu_f} \frac{1}{Re} \nabla^2 \mathbf{V} + \frac{(\rho\beta)_{nf}}{\rho_{nf} \beta_f} Ri \theta_{nf} + \frac{\rho_f \sigma_{nf}}{\rho_{nf} \sigma_f} \mathbf{V} \times \mathbf{B}^*, \quad (18)$$

$$\mathbf{V} \nabla \theta_{nf} = \frac{(\rho C_p)_f}{(\rho C_p)_{nf}} \frac{k_{nf}}{k_f} \frac{1}{Re Pr} \nabla^2 \theta_{nf} + \frac{(\rho C_p)_f}{(\rho C_p)_{nf}} \frac{D_B^*}{Re Pr Le} \nabla \varphi^* \nabla \theta_{nf}$$

$$+ \frac{(\rho C_p)_f}{(\rho C_p)_{nf}} \frac{D_T^*}{Re Pr Le N_{BT}} \frac{\nabla \theta_{nf} \nabla \theta_{nf}}{1 + \delta \theta_{nf}}, \quad (19)$$

$$\mathbf{V} \nabla \varphi^* = \frac{D_B^*}{Re Sc} \nabla^2 \varphi^* + \frac{D_T^*}{Re Sc N_{BT}} \frac{\nabla^2 \theta_{nf}}{1 + \delta \theta_{nf}}, \quad (20)$$

$$\nabla \theta_w = 0, \quad (21)$$

subject to the dimensionless boundary conditions.

On the bottom wall:

$$U = V = 0, \quad \frac{\partial \varphi^*}{\partial n} = -\frac{D_T^*}{D_B^*} \frac{1}{N_{BT}} \frac{1}{1 + \delta \theta_{nf}} \frac{\partial \theta_{nf}}{\partial n}, \quad \theta_{nf} = 1, \quad (\text{heated section}) \quad (22)$$

$$U = V = 0, \quad \frac{\partial \varphi^*}{\partial n} = 0, \quad \frac{\partial \theta_{nf}}{\partial n} = 0, \quad (\text{remaining adiabatic section}) \quad (23)$$

On the cold left and right vertical walls:

$$U = V = 0, \quad \frac{\partial \varphi^*}{\partial n} = -\frac{D_T^*}{D_B^*} \frac{1}{N_{BT}} \frac{1}{1 + \delta \theta_{nf}} \frac{\partial \theta_{nf}}{\partial n}, \quad \theta_{nf} = 0, \quad (24)$$

On the horizontal adiabatic moving top wall:

$$U = 1, \quad V = 0, \quad \frac{\partial \varphi^*}{\partial n} = 0, \quad \frac{\partial \theta_{nf}}{\partial n} = 0, \quad (25)$$

On the trapezoidal solid body's walls:

$$\theta_{nf} = \theta_w, \quad (26)$$

$$U = V = 0, \quad \frac{\partial \varphi^*}{\partial n} = -\frac{D_T^*}{D_B^*} \frac{1}{N_{BT}} \frac{1}{1 + \delta \theta_{nf}} \frac{\partial \theta_{nf}}{\partial n}, \quad \frac{\partial \theta_{nf}}{\partial n} = K_r \frac{\partial \theta_w}{\partial n}. \quad (27)$$

Here, $\mathbf{V} = (U_0, V_0)$ and $\mathbf{B}^* = (Ha^2 \sin \gamma, Ha^2 \cos \gamma)$. The reference Brownian diffusion and thermophoretic diffusion coefficients are $D_{B0} = k_b T_c / 3\pi \mu_f d_p$ and $D_{T0} = 0.26(k_f / (2k_f + k_p))(\mu_f / \rho_f \theta) \phi$, respectively. The diffusivity ratio parameter (Brownian diffusivity/thermophoretic diffusivity) is $N_{BT} = \phi D_{B0} T_c / D_{T0} (T_h - T_c)$. The other parameters are Grashof number $Gr = g \beta_f (T_h - T_c) L^3 / \nu_f^2$, Hartmann number $Ha = \mathbf{BL} \sqrt{(\sigma_f / \mu_f)}$, Lewis number $Le = k_f / (\rho C_p)_f \phi D_{B0}$, Prandtl number $Pr = \nu_f / \alpha_f$, Reynolds number $Re = U_0 L / \nu_f$, Richardson number $Ri = Gr / Re^2$, Schmidt number $Sc = \nu_f / D_{B0}$. In (27), the thermal conductivity ratio K_r is k_w / k_{nf} . Both the local and average Nusselt numbers at the heated part of the bottom wall can be evaluated, respectively, using

$$Nu_{nf} = - \left(\frac{\partial \theta_{nf}}{\partial Y} \right)_{Y=0}, \quad \overline{Nu}_{nf} = \int_{\frac{1-H}{2}}^{\frac{1+H}{2}} Nu_{nf} dX. \quad (28)$$

3. Numerical Method and Validation

We used the Galerkin weighted residual finite element method to solve problems (17)–(27). The reader is referred to Alsabery et al. [34] for a brief description of the method. For convergence of the solution, we used the convergence criterion $|(\Gamma^{i+1} - \Gamma^i)/\Gamma^{i+1}| \leq 10^{-6}$, where Γ represents the variable and i is the iteration number. The ranges of values of the Reynolds number and Richardson number considered in the current work held the nanofluid flow to be incompressible and laminar.

First we validated the present code against the experimental and numerical work of Calcagni et al. [35]. Figure 2 presents the results of streamlines and isotherms for the case where there was no solid body in the cavity. Very good agreement was demonstrated between our results and the experimental and numerical results of Calcagni et al. [35]. Next, we considered the case of natural convection in a Buongiorno's nanofluid-filled cavity. Figure 3 shows a comparison of our calculated average Nusselt number to that of the experimental work of Ho et al. [36] and the numerical results of Sheikhzadeh et al. [37] and Motlagh and Soltanipour [38]. We can see that a reasonably good agreement was reached. Figure 4 further shows a good agreement between the present method and the numerical results of Corcione et al. [39] for the streamlines, isotherms, and nanoparticle distribution of natural convection. Finally, we can see from Figure 5 that our calculated thermal conductivity and dynamic viscosity compare reasonably well with the results of Chon et al. [40] and Corcione et al. [39] and Ho et al. [36] and Corcione et al. [39], respectively.

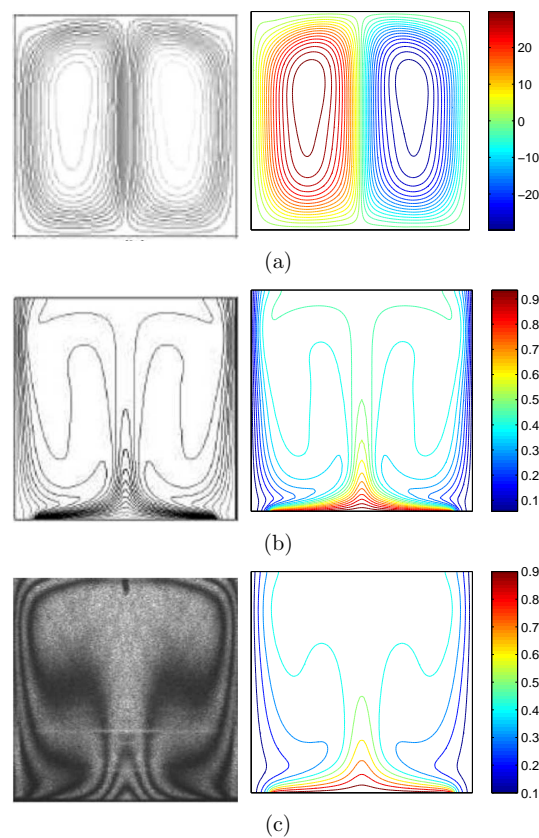


Figure 2. (left) Numerical results from Calcagni et al. [35] and (right) the present study for (a) streamlines at $Ra = 10^6$ and $H = 0.4$; (b) isotherms at $Ra = 10^5$ and $H = 0.8$; and (c) (left) experimental results [35] and (right) present numerical results for isotherms at $Ra = 1.836 \times 10^5$ and $H = 0.8$ for the case where $\phi = 0$ and $D = 0$.

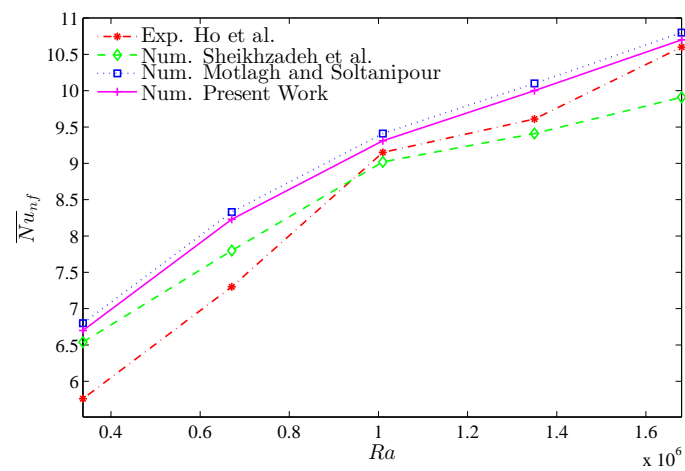


Figure 3. Comparison between the experimental and numerical results for the average Nusselt number for different values of the Rayleigh number.

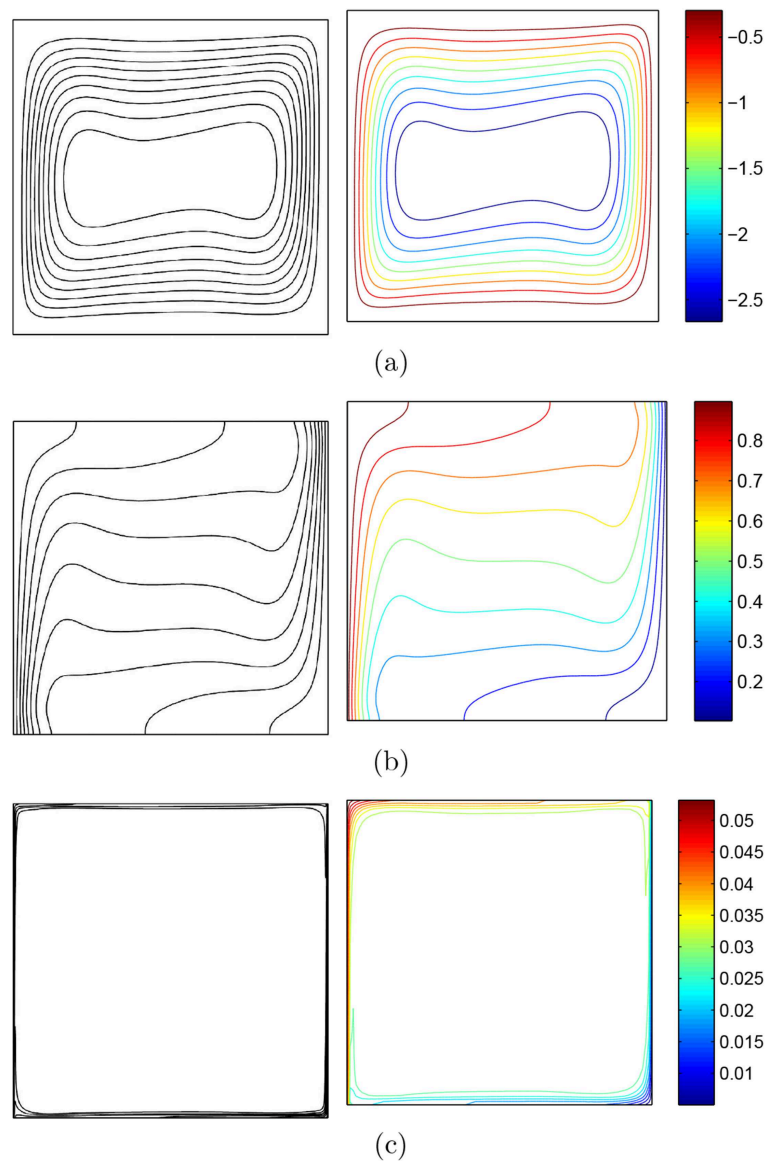


Figure 4. (left) Corcione et al. [39] vs. (right) present study: (a) streamlines; (b) isotherms; and (c) nanoparticle distribution for the case where $Ra = 3.37 \times 10^5$, $\phi = 0.04$, and $D = 0$.

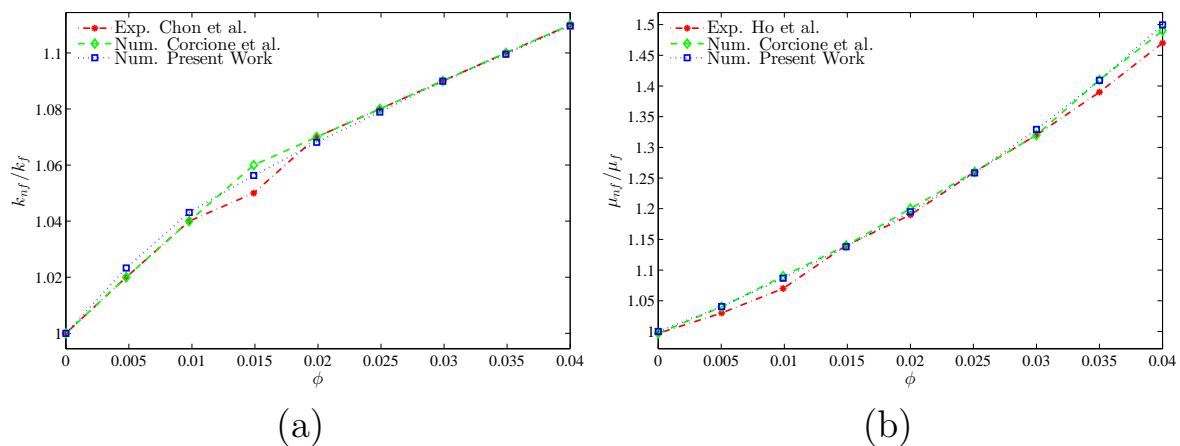


Figure 5. (a) Thermal conductivity ratio: present work vs. Chon et al. [40] and Corcione et al. [39]; (b) Dynamic viscosity ratio: present work vs. Ho et al. [36] and Corcione et al. [39].

4. Results and Discussion

We investigated the effects of the Richardson number (Ri), Hartmann number (Ha), nanoparticle volume fraction (ϕ), and the height of the trapezoidal body (D) on the streamlines, isotherms, nanoparticle distribution, and local and average Nusselt numbers. The other parameters were fixed as follows: $Re = 100$, $Pr = 4.623$, $H = 0.5$, $Le = 3.5 \times 10^5$, $Sc = 3.55 \times 10^4$, $\gamma = \pi/4$, $N_{BT} = 1.1$, and $\delta = 155$. The trapezoidal body was assumed to be made of fiberglass with $k_w = 0.045 \text{ W/(m K)}$. Table 1 lists the thermophysical properties of the Al_2O_3 -water nanofluid.

Table 1. Thermophysical properties of the Al_2O_3 -water at $T = 310 \text{ K}$ [38,41].

| Physical Properties | Fluid Phase (Water) | Al_2O_3 |
|---------------------------------------|---------------------|-------------------------|
| C_p (J/kgK) | 4178 | 765 |
| ρ (kg/m^3) | 993 | 3970 |
| k ($\text{Wm}^{-1}\text{K}^{-1}$) | 0.628 | 40 |
| $\beta \times 10^5$ (1/K) | 36.2 | 0.85 |
| $\mu \times 10^6$ (kg/ms) | 695 | – |
| d_p (nm) | 0.385 | 33 |

Figure 6 describes the fluid flow (streamlines), temperature fields (isothermal lines), and nanoparticle distribution (volume fraction distribution) for several Ri , while the other parameters were fixed at $Ha = 20$, $\phi = 0.02$ and $D = 0.3$. The flow within the square cavity takes a singular streamline cell that rotates clockwise next to the top moving wall. Most of the isotherms follow vertical lines close to the right cold wall; such a behaviour is clearly related to the dominant forced convection. This phenomenon can be obviously observed from the contours of the nanoparticle distribution; most of the nanoparticle concentration appears at the lower segment of the square cavity affected by the movement of the driven top wall. Increasing the Richardson number clearly affects the flow behaviour. A secondary streamline cell in the anticlockwise direction takes place at the lower part of the cavity near to the right wall. The strength of the streamlines is enhanced by the augmentation of Ri . This indicates that natural convection is dominant. The isotherm patterns transfer from the vertical shape into a plume-like pattern with high destruction within the middle of the cavity. The concentration of nanoparticles moves around the walls of the cavity which clearly shows the enhancement of the thermophoresis effects, as depicted in Figure 6c,d.

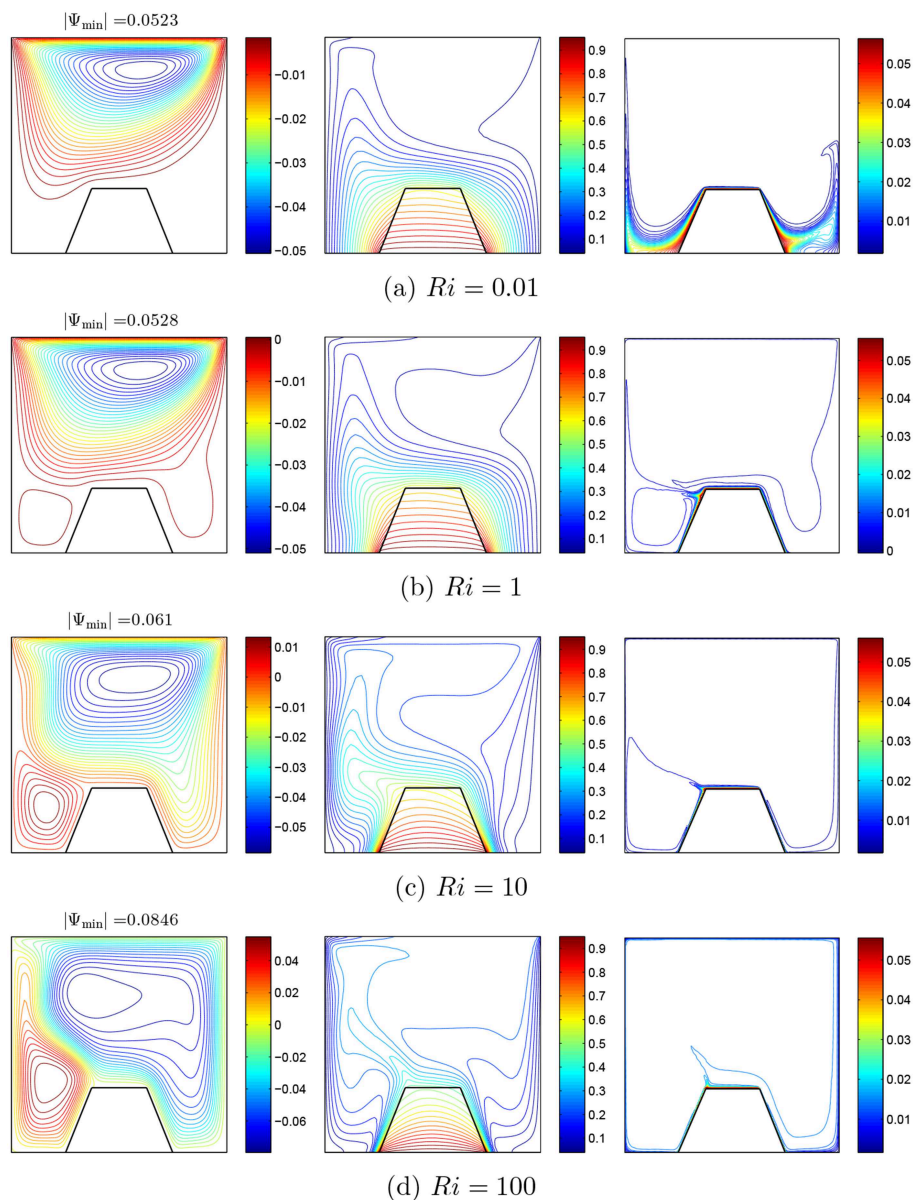


Figure 6. Effects of the Richardson number (Ri) on the streamlines (left), isotherms (middle), and nanoparticle distribution (right) for $Ha = 20$, $\phi = 0.02$, and $D = 0.3$.

Figure 7 examines the effect of the Hartmann number (Ha) on the streamlines, isotherms, and nanoparticle distribution for fixed values of $Ri = 10$, $\phi = 0.02$, and $D = 0.3$. The flow within the square cavity appears with two streamline circular cells in different directions, one at the upper part and the other at the lower part next to the right wall for the case where $Ha = 0$. The isotherm patterns are destroyed at the left segment of the considered cavity. The nanoparticle distributions seem to be clearly affected by the dragging force that is supported by the convection heat transfer; the distribution of nanoparticles takes place around the trapezoidal body next to the walls of the cavity. The magnetic field reduces the buoyancy and inertial forces; as a result, the strength of the flow circulation decreases. This application of Ha leads to an inhibition of the thermal gradient, the isotherms pattern show less distortion, and more lines transfer to the right segment of the cavity. The increase in Ha shows an enhancement in the distribution of the nanoparticles which leads to a significant nanoparticle migration. Increasing the Hartmann number up to the higher value ($Ha = 50$) clearly affects the flow circulation; a third streamline cell appears at the lower right part of the cavity, as observed in Figure 7d.

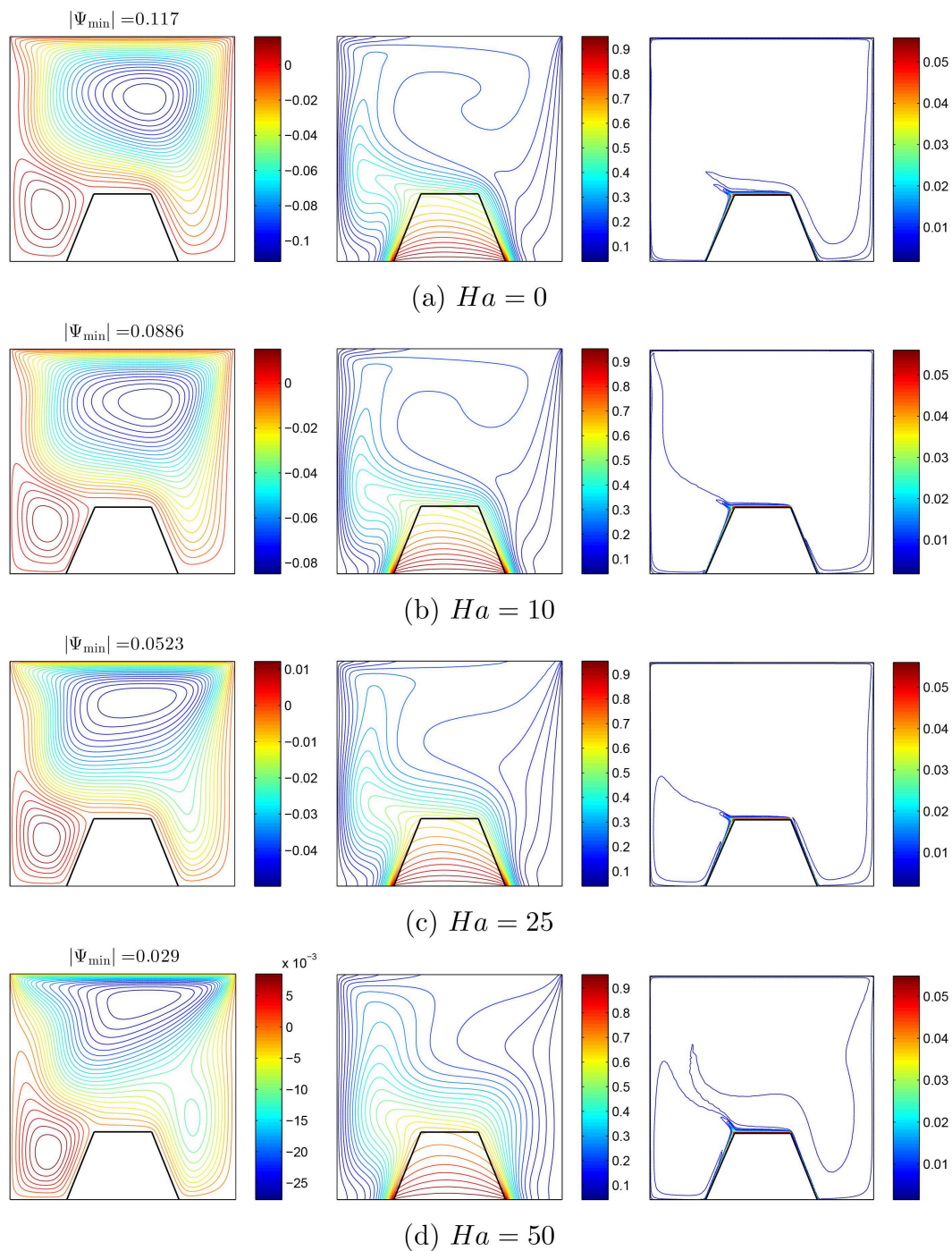


Figure 7. Effects of the Hartmann number (Ha) on the streamlines (left), isotherms (middle), and nanoparticle distribution (right) for $Ri = 10$, $\phi = 0.02$, and $D = 0.3$.

The impacts of the solid volume fraction (ϕ) on the streamlines, isotherms, and nanoparticle distribution are described in Figure 8 for $Ri = 10$, $Ha = 15$ and $D = 0.3$. The flow circulation shows less enhancement as the solid volume fraction increases; however, the strength of the flow circulation increases, which is clearly related to the nanoparticle Brownian diffusion. The isotherm lines show more deterioration and more lines move to the left wall, which is evidence of the temperature gradient increment. The temperature gradient leads to an increment in the thermophoresis; the nanoparticles show high distribution next to the right cold wall. The Brownian movements increase with such a loading of nanoparticles; nanoparticle migration mostly occurs close to the trapezoidal solid body.

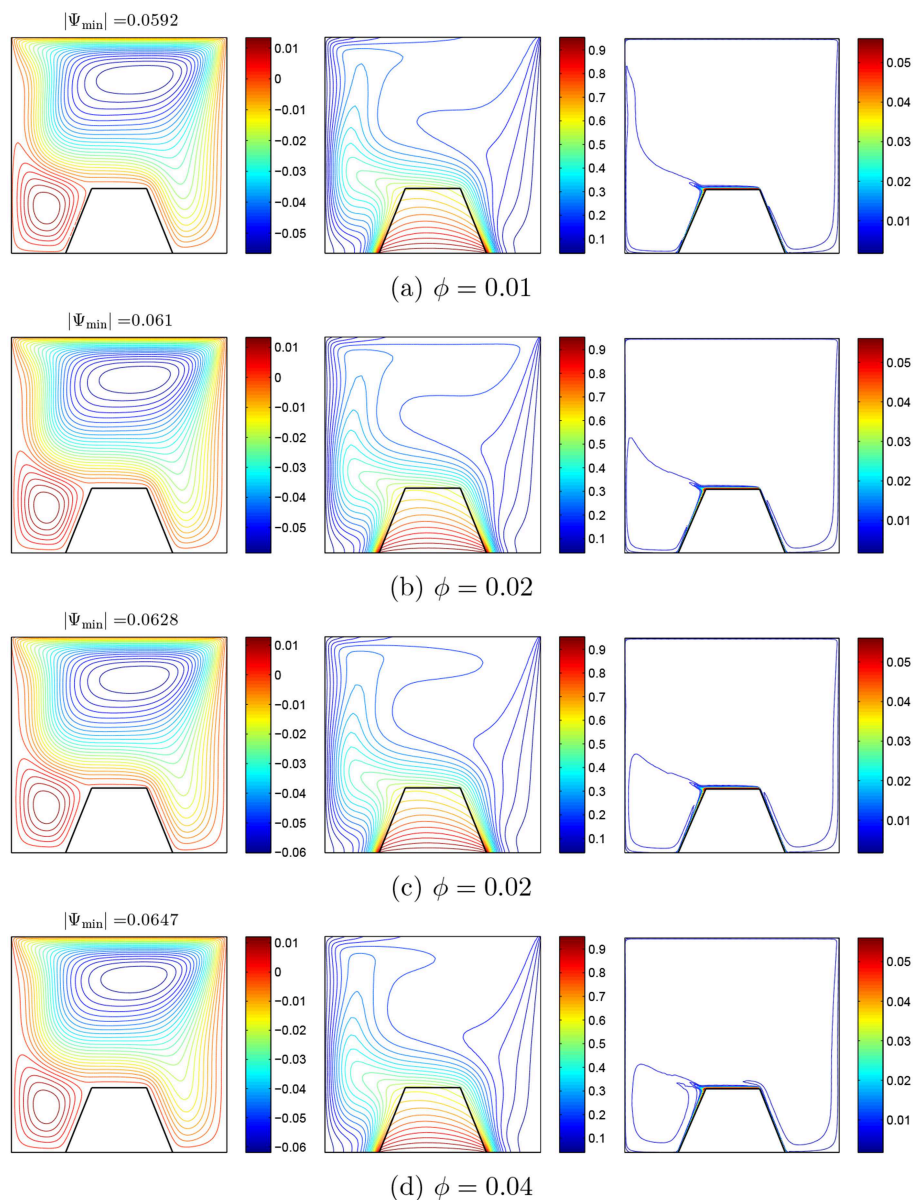


Figure 8. Effects of the solid volume fraction (ϕ) on the streamlines (left), isotherms (middle), and nanoparticle distribution (right) for $Ri = 10$, $Ha = 15$, and $D = 0.3$.

The effects of the length of the bottom base of the trapezoidal body (D) on the streamlines, isotherms, and nanoparticle distribution are depicted in Figure 9 for $Ri = 10$, $Ha = 20$ and $\phi = 0.02$. The lower length of the trapezoidal body ($D = 0.15$) shows a big area for the nanofluid circulation; as a result, a high buoyancy and inertial forces occur. The isotherm patterns appear mostly distorted close to the left vertical wall due to the high thermal gradient. Strong distribution occurs on the contours of the nanoparticles; most of the nanoparticles are distributed at the lower segment of the cavity. Increasing D tends to reduce the flow circulation area and the buoyancy effect which clearly tends to decrease the strength of the flow circulation, as demonstrated in Figure 9c,d. The deterioration of the isotherms reduces and more heat moves to the right segment of the cavity. This is related to the reduction of the thermal gradient affected by the low thermal conductivity of the solid trapezoidal body. Imposing a big solid trapezoidal body tends to reduce the nanoparticle distribution which clearly leads to more nanoparticles migration within the square cavity.

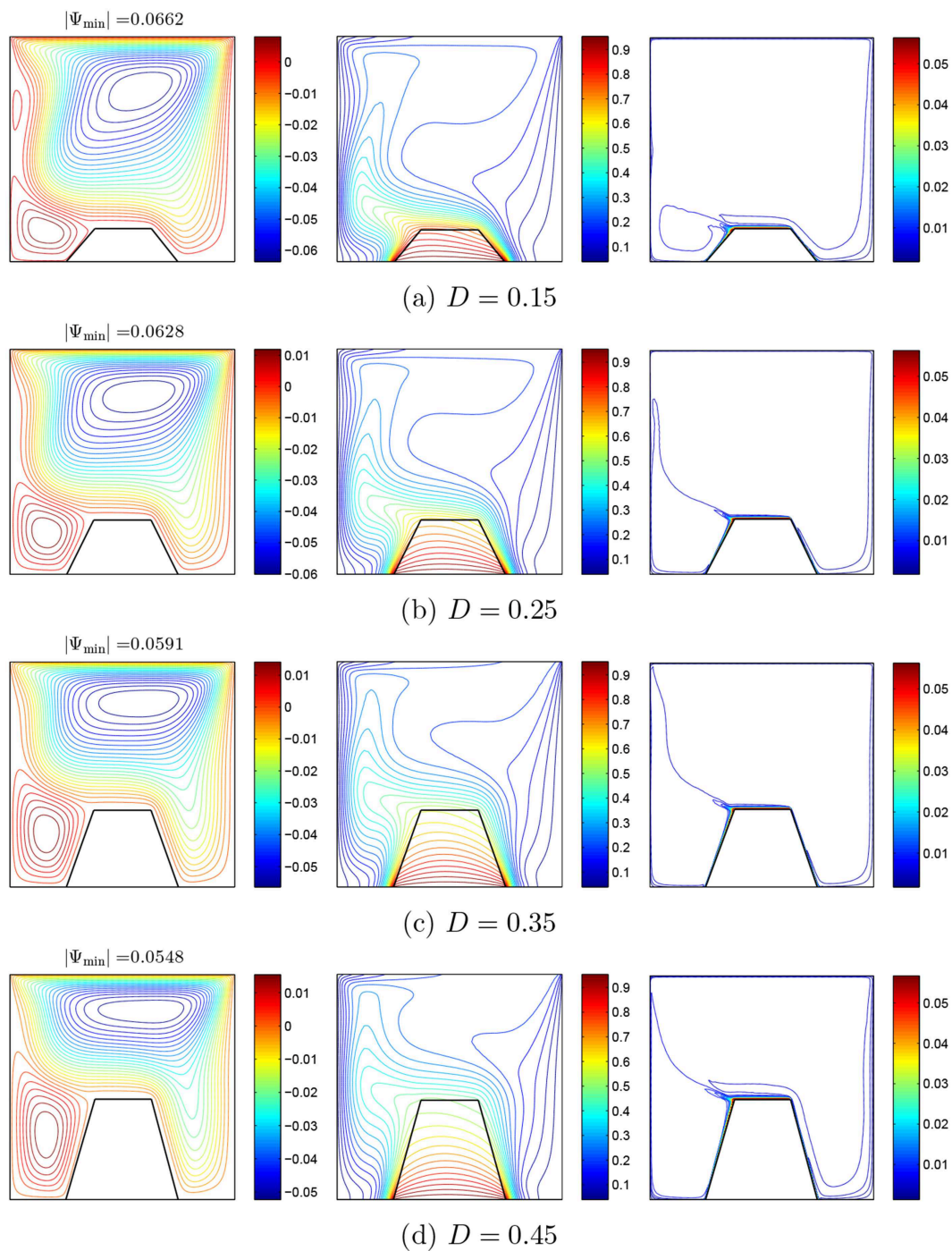


Figure 9. Effects of the trapezoidal body (D) on the streamlines (left), isotherms (middle), and nanoparticle distribution (right) for $Ri = 10$, $Ha = 20$, and $\phi = 0.02$.

Figure 10 shows the impact of the Richardson and Hartmann numbers on the interface of the local Nusselt numbers with X at the heated part of the bottom wall for $\phi = 0.02$ and $D = 0.3$. The local heat transfer enhances with an augmentation of the Richardson number due to the high buoyancy effect which results in an increase in the thermal gradient, as shown in Figure 10a. Figure 10b presents the effect of the Hartmann number on the local heat transfer. As observed from this figure, an increase in Ha tends to reduce the local Nusselt number due to the reduced thermal gradient and Brownian diffusion.

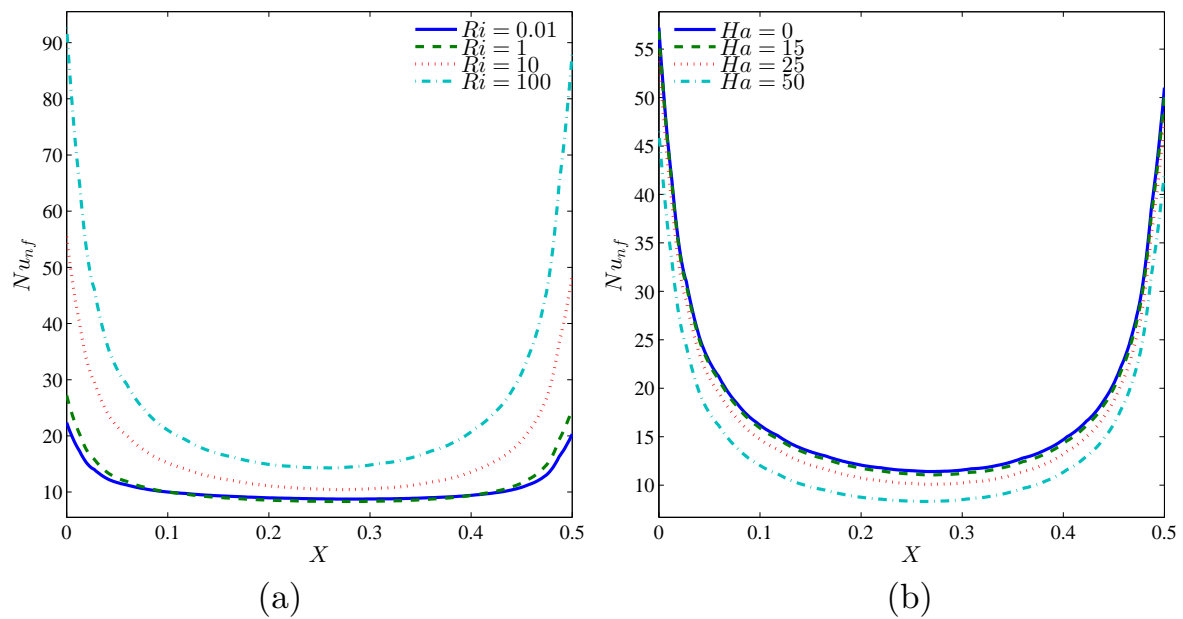


Figure 10. Plots of the local Nusselt number vs. X for different (a) Ri and (b) Ha at $\phi = 0.02$ and $D = 0.3$.

The effect of the nanoparticle loading on the interface of the local Nusselt numbers with X for $Ri = 10$, $Ha = 20$, and $D = 0.3$ is described in Figure 11a. The local Nusselt number is an increasing function of the solid volume fraction due to the increment of the thermal gradient due to an addition of the nanoparticles. Such a behaviour is related to the enhancement of the Brownian diffusion and the thermophoresis effects. Figure 11b depicts the influence of the local heat transfer for different lengths of the trapezoidal body at $Ri = 10$, $Ha = 20$, and $\phi = 0.02$. At the left segment of the cavity, the local Nusselt number shows a clear reduction with an increment in D , while this increment in D tends to enhance the local Nusselt number at the right segment of the cavity, which results in an increase of the thermal gradient.

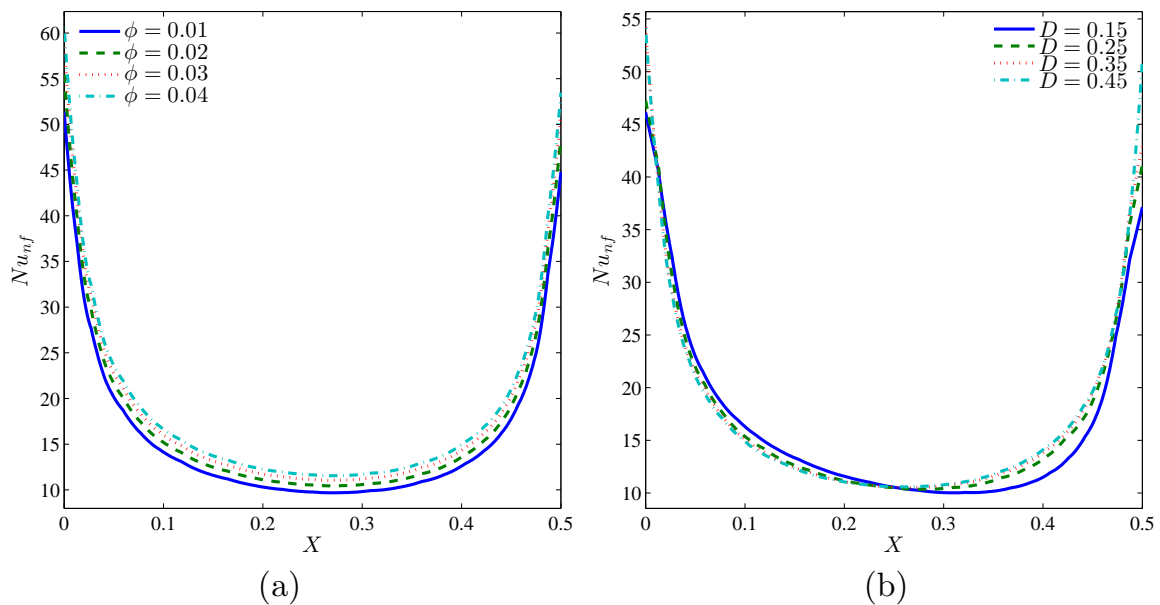


Figure 11. Plots of the local Nusselt number vs. X for different (a) ϕ and (b) D at $Ri = 10$ and $Ha = 20$.

Figure 12 shows the variation in the average Nusselt number with various solid volume fractions (ϕ) and Richardson numbers (Ri) for $Ha = 20$ and $D = 0.3$. At a low value of the Richardson number ($Ri = 0.01$), when the forced convection is dominant, the convection heat transfer shows very clear enhancement with the addition of the solid volume fraction. This happens due to the increment of the thermal conductivity and thermophoresis. The augmentation of Ri leads to the enhancement of the thermophoresis effects, and as a result, the convection heat transfer increases. More importantly, when Ri is relatively high ($Ri = 10$ and 100), the addition of the solid volume fraction that exceeds 0.035 leads to a reduction in the average Nusselt number. This happens due to the fact that the buoyancy effects dominate the thermal conductivity and thermophoresis effects at this stage.

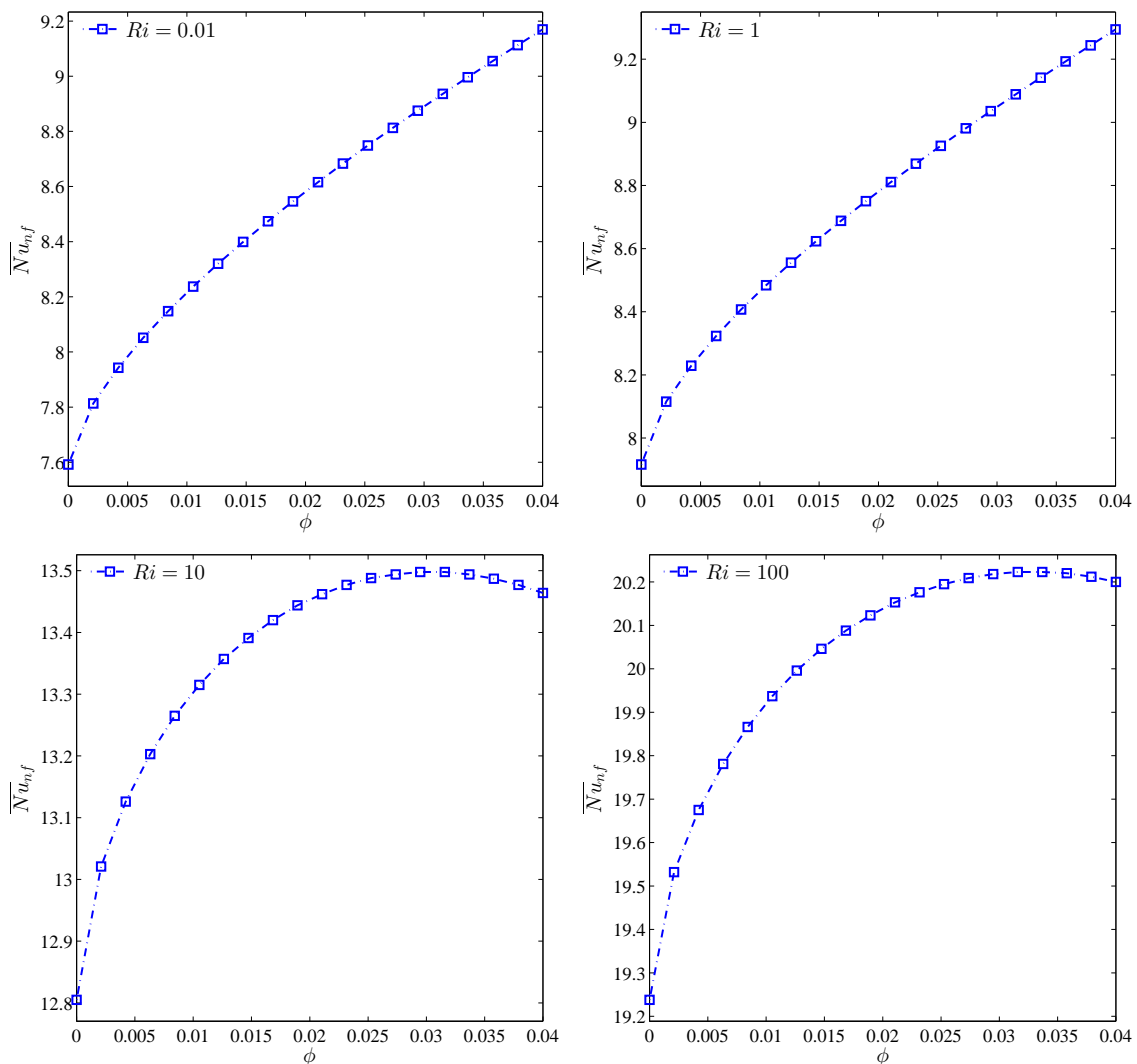


Figure 12. Plots of the average Nusselt number vs. ϕ for different Ri at $Ha = 20$ and $D = 0.3$.

The variation in the average Nusselt number with the Hartmann number (Ha) and the solid volume fraction (ϕ) for $Ri = 10$ and $D = 0.3$ are shown in Figure 13. Clearly, we can see the enhancement of the convection heat transfer with an increment in the nanoparticle loading. This is due to the increase in the thermal conductivity which leads to a rise in the thermal gradient. However, the increasing of the solid volume fraction that exceed 0.03 tends to decrease the average Nusselt number. Imposing an external magnetic field $Ha > 0$ leads to an obvious reduction in the rate of the heat transfer, which is due to the thermal gradient diminishing.

Figure 14a describes the influence of the solid volume fraction (ϕ) on the average Nusselt number for various values of the Richardson number and $Ha = 20$ and $D = 0.3$. The convection heat transfer enhances with an augmentation of Ri , which is due to the increase in the buoyancy and the shear forces. The nanoparticle loading shows an improvement in the average Nusselt number due to the thermal conductivity and thermophoresis increment. However, the convection heat transfer shows a reduction behaviour when the augmentation of the solid volume fraction exceeds 0.03. The effects of ϕ on the average Nusselt number for various values of the Hartmann number (Ha) are described in Figure 14b for $Ri = 10$ and $D = 0.3$. A decreasing behaviour is observed for the average Nusselt number with an increment in the Hartmann number due the the reduction in the thermal gradient with as Ha increases.

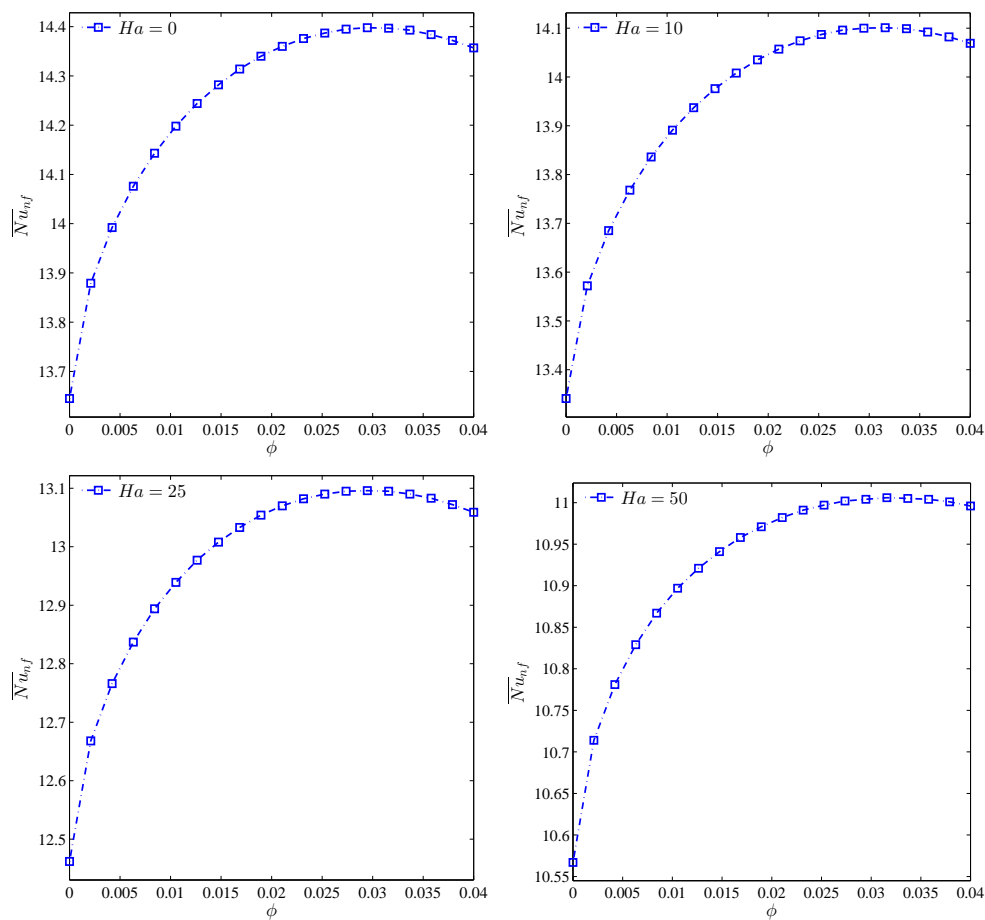


Figure 13. Plots of the average Nusselt number vs. ϕ for different Ha at $Ri = 10$ and $D = 0.3$.

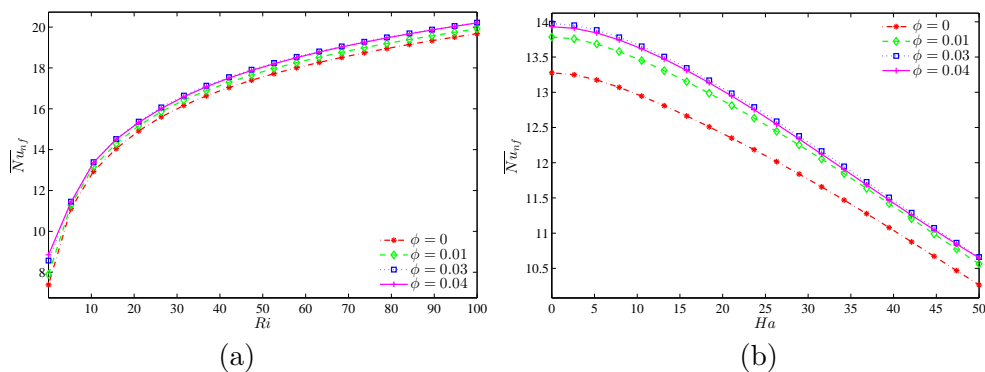


Figure 14. Plots of the average Nusselt number vs. (a) Ri and (b) Ha for different ϕ at $D = 0.3$.

The effects of the length of the bottom base of the trapezoidal solid body (D) on the average Nusselt number for various values of the Hartmann number are shown in Figure 15a. The convection heat transfer reduces with an increase in the Hartmann number. Inserting a slight solid body within the square cavity leads to an enhancement in the rate of heat transfer. This behaviour is seen for a low magnetic field ($Ha < 10$). However, a different behaviour is obtained for the convection heat transfer when the magnetic field exceeds 25. The average Nusselt number enhances with as D increases. Figure 15b shows that the average Nusselt number appears to have an enhancement behaviour with as D increases for relatively low $\phi \leq 0.025$.

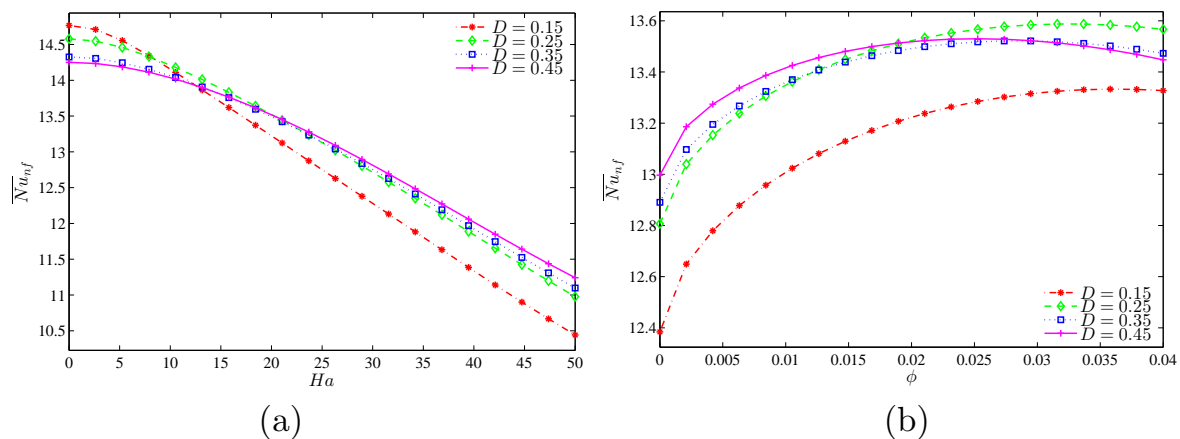


Figure 15. Variation in the average Nusselt number with (a) Ha and (b) ϕ for different D at $Ri = 10$.

5. Conclusions

The current paper investigated the effects of a magnetic field on mixed convective heat transfer in an Al_2O_3 –water nanofluid filled lid-driven square cavity with a bottom trapezoidal solid body. Buongiorno’s two-phase model was adopted, i.e., the slip between the base fluid and the nanoparticles was taken into consideration. The governing equations were made dimensionless and then solved using the Galerkin weighted residual finite element method. The concluding remarks are as follows:

1. At a high Richardson number when the natural convection is dominant, thermophoresis can produce a homogeneous dispersion of nanoparticles.
2. The convection heat transfer enhances with the nanoparticle volume fraction and is affected by increments in the thermal conductivity and thermophoresis. In contrast, at a high Richardson number, a boost in the nanoparticle volume fraction that exceeds 0.035 leads to a reduction in the average Nusselt number.
3. A cavity with small trapezoidal solid body and low magnetic field tends to show more enhancement on the rate of heat transfer. However, imposing a high magnetic field in a cavity with a big trapezoidal solid body leads to the best improvement in convection heat transfer.
4. A strong enhancement of the average Nusselt number occurs with a high nanoparticle volume fraction and a relatively small trapezoidal solid body.
5. Thermophoresis and Brownian motion effects play significant roles in the augmentation of convection heat transfer.

Author Contributions: Conceptualization, M.A.S., A.I.A. and I.H.; Methodology, M.A.S. and A.I.A.; Validation, A.I.A.; Analysis, M.A.S., A.I.A. and I.H.

Funding: The work was supported by DCC-KFUPM grant IN171023.

Acknowledgments: We thank the respected reviewers for their constructive comments which clearly enhanced the quality of the manuscript.

Conflicts of Interest: The authors declare that there is no conflict of interest.

Abbreviations

The following abbreviations are used in this manuscript:

| | |
|-----------------|---|
| \vec{B} | applied magnetic field |
| B | magnitude of magnetic field |
| C_p | specific heat capacity |
| d_f | diameter of the base fluid molecule |
| d_p | diameter of the nanoparticle |
| D | dimensionless length of the trapezoidal solid body, $D = d/L$ |
| D_B | Brownian diffusion coefficient |
| D_{B0} | reference Brownian diffusion coefficient |
| D_T | thermophoretic diffusivity coefficient |
| D_{T0} | reference thermophoretic diffusion coefficient |
| g | gravitational acceleration |
| H | dimensionless width of the trapezoidal solid body, $H = h/L$ |
| Ha | Hartmann number |
| Gr | Grashof number |
| k | thermal conductivity |
| K_r | square wall to nanofluid thermal conductivity ratio, $K_r = k_w/k_{nf}$ |
| L | width and height of enclosure |
| Le | Lewis number |
| N_{BT} | ratio of Brownian to thermophoretic diffusivity |
| \overline{Nu} | average Nusselt number |
| Pr | Prandtl number |
| Re | Reynolds number |
| Re_B | Brownian motion Reynolds number |
| Ri | Richardson number, $Ri = Gr/Re^2$ |
| Sc | Schmidt number |
| T | temperature |
| T_0 | reference temperature (310K) |
| T_{fr} | freezing point of the base fluid (273.15K) |
| u, v | velocity components in the x and y directions, respectively |
| U, V | dimensionless velocity components in the X and Y directions, respectively |
| u_B | Brownian velocity of the nanoparticle |
| x, y & X, Y | space coordinates & dimensionless space coordinates |
| Greek symbols | |
| α | thermal diffusivity |
| γ | inclination angle of magnetic field |
| β | thermal expansion coefficient |
| δ | normalized temperature parameter |
| θ | dimensionless temperature |
| μ | dynamic viscosity |
| ν | kinematic viscosity |
| ρ | density |
| σ | electrical conductivity |
| φ | solid volume fraction |
| φ^* | normalized solid volume fraction |
| ϕ | average solid volume fraction |
| Subscript | |
| b | bottom wall |
| c | cold |
| f | base fluid |
| h | hot |
| nf | nanofluid |
| p | solid nanoparticles |
| t | top wall |
| w | trapezoidal solid wall |

References

1. Alsabery, A.I.; Tayebi, T.; Chamkha, A.J.; Hashim, I. Effects of non-homogeneous nanofluid model on natural convection in a square cavity in the presence of conducting solid block and corner heater. *Energies* **2018**, *11*, 2507. [[CrossRef](#)]
2. Gibanov, N.S.; Sheremet, M.A.; Oztop, H.F.; Abu-Hamdeh, N. Mixed convection with entropy generation of nanofluid in a lid-driven cavity under the effects of a heat-conducting solid wall and vertical temperature gradient. *Eur. J. Mech. B/Fluids* **2018**, *70*, 148–159. [[CrossRef](#)]
3. Torrance, K.; Davis, R.; Eike, K.; Gill, P.; Gutman, D.; Hsui, A.; Lyons, S.; Zien, H. Cavity flows driven by buoyancy and shear. *J. Fluid Mech.* **1972**, *51*, 221–231. [[CrossRef](#)]
4. Moallemi, M.K.; Jang, K.S. Prandtl number effects on laminar mixed convection heat transfer in a lid-driven cavity. *Int. J. Heat Mass Transf.* **1992**, *35*, 1881–1892. [[CrossRef](#)]
5. Oztop, H.F.; Dagtekin, I. Mixed convection in two-sided lid-driven differentially heated square cavity. *Int. J. Heat Mass Transf.* **2004**, *47*, 1761–1769. [[CrossRef](#)]
6. Al-Amiri, A.M.; Khanafer, K.M.; Pop, I. Numerical simulation of combined thermal and mass transport in a square lid-driven cavity. *Int. J. Therm. Sci.* **2007**, *46*, 662–671. [[CrossRef](#)]
7. Sharif, M.A.R. Laminar mixed convection in shallow inclined driven cavities with hot moving lid on top and cooled from bottom. *Appl. Therm. Eng.* **2007**, *27*, 1036–1042. [[CrossRef](#)]
8. Ismael, M.A.; Pop, I.; Chamkha, A.J. Mixed convection in a lid-driven square cavity with partial slip. *Int. J. Therm. Sci.* **2014**, *82*, 47–61. [[CrossRef](#)]
9. Ismael, M.A. Numerical solution of mixed convection in a lid-driven cavity with arc-shaped moving wall. *Eng. Comput.* **2017**, *34*, 869–891. [[CrossRef](#)]
10. Tiwari, R.K.; Das, M.K. Heat transfer augmentation in a two-sided lid-driven differentially heated square cavity utilizing nanofluids. *Int. J. Heat Mass Transf.* **2007**, *50*, 2002–2018. [[CrossRef](#)]
11. Talebi, F.; Mahmoudi, A.H.; Shahi, M. Numerical study of mixed convection flows in a square lid-driven cavity utilizing nanofluid. *Int. Commun. Heat Mass Transf.* **2010**, *37*, 79–90. [[CrossRef](#)]
12. Chamkha, A.J.; Abu-Nada, E. Mixed convection flow in single-and double-lid driven square cavities filled with water- Al_2O_3 nanofluid: Effect of viscosity models. *Eur. J. Mech. B/Fluids* **2012**, *36*, 82–96. [[CrossRef](#)]
13. Karimipour, A.; Esfe, M.H.; Safaei, M.R.; Semiromi, D.T.; Jafari, S.; Kazi, S. Mixed convection of copper-water nanofluid in a shallow inclined lid driven cavity using the lattice Boltzmann method. *Phys. A Stat. Mech. Appl.* **2014**, *402*, 150–168. [[CrossRef](#)]
14. Alsabery, A.I.; Hashim, I.; Chamkha, A.J.; Saleh, H.; Chanane, B. Effect of spatial side-wall temperature variation on transient natural convection of a nanofluid in a trapezoidal cavity. *Int. J. Numer. Methods Heat Fluid Flow* **2017**, *27*, 1365–1384. [[CrossRef](#)]
15. Wen, D.; Ding, Y. Experimental investigation into convective heat transfer of nanofluids at the entrance region under laminar flow conditions. *Int. J. Heat Mass Transf.* **2004**, *47*, 5181–5188. [[CrossRef](#)]
16. Buongiorno, J. Convective transport in nanofluids. *J. Heat Transf.* **2006**, *128*, 240–250. [[CrossRef](#)]
17. Alinia, M.; Ganji, D.; Gorji-Bandpy, M. Numerical study of mixed convection in an inclined two sided lid driven cavity filled with nanofluid using two-phase mixture model. *Int. Commun. Heat Mass Transf.* **2011**, *38*, 1428–1435. [[CrossRef](#)]
18. Sheikholeslami, M.; Gorji-Bandpy, M.; Ganji, D.D.; Soleimani, S. Thermal management for free convection of nanofluid using two phase model. *J. Mol. Liquids* **2014**, *194*, 179–187. [[CrossRef](#)]
19. Sheremet, M.A.; Pop, I. Mixed convection in a lid-driven square cavity filled by a nanofluid: Buongiorno's mathematical model. *Appl. Math. Comput.* **2015**, *266*, 792–808. [[CrossRef](#)]
20. Malvandi, A.; Ganji, D.D. Mixed convection of alumina/water nanofluid in microchannels using modified Buongiorno's model in presence of heat source/sink. *J. Appl. Fluid Mech.* **2016**, *9*, 2277–2289. [[CrossRef](#)]
21. Garoosi, F.; Talebi, F. Numerical analysis of conjugate natural and mixed convection heat transfer of nanofluids in a square cavity using the two-phase method. *Adv. Powder Technol.* **2017**, *28*, 1668–1695. [[CrossRef](#)]
22. Alsabery, A.I.; Ismael, M.A.; Chamkha, A.J.; Hashim, I. Mixed convection of Al_2O_3 -water nanofluid in a double lid-driven square cavity with a solid inner insert using Buongiorno's two-phase model. *Int. J. Heat Mass Transf.* **2018**, *119*, 939–961. [[CrossRef](#)]

23. Nkurikiyimfura, I.; Wang, Y.; Pan, Z. Heat transfer enhancement by magnetic nanofluids—A review. *Renew. Sustain. Energy Rev.* **2013**, *21*, 548–561. [[CrossRef](#)]
24. Alsabery, A.I.; Sheremet, M.A.; Chamkha, A.J.; Hashim, I. MHD convective heat transfer in a discretely heated square cavity with conductive inner block using two-phase nanofluid model. *Sci. Rep.* **2018**, *8*, 7410. [[CrossRef](#)] [[PubMed](#)]
25. Chamkha, A.J. Hydromagnetic combined convection flow in a vertical lid-driven cavity with internal heat generation or absorption. *Numer. Heat Transf. Part A Appl.* **2002**, *41*, 529–546. [[CrossRef](#)]
26. Öztop, H.F.; Al-Salem, K.; Pop, I. MHD mixed convection in a lid-driven cavity with corner heater. *Int. J. Heat Mass Transf.* **2011**, *54*, 3494–3504. [[CrossRef](#)]
27. Chatterjee, D. MHD mixed convection in a lid-driven cavity including a heated source. *Numer. Heat Transf. Part A Appl.* **2013**, *64*, 235–254. [[CrossRef](#)]
28. Selimefendigil, F.; Öztop, H.F.; Chamkha, A.J. MHD mixed convection and entropy generation of nanofluid filled lid driven cavity under the influence of inclined magnetic fields imposed to its upper and lower diagonal triangular domains. *J. Magn. Magn. Mater.* **2016**, *406*, 266–281. [[CrossRef](#)]
29. Öztop, H.F.; Sakhrieh, A.; Abu-Nada, E.; Al-Salem, K. Mixed convection of MHD flow in nanofluid filled and partially heated wavy walled lid-driven enclosure. *Int. Commun. Heat Mass Transf.* **2017**, *86*, 42–51. [[CrossRef](#)]
30. Chamkha, A.J.; Rashad, A.M.; Armaghani, T.; Mansour, M.A. Effects of partial slip on entropy generation and MHD combined convection in a lid-driven porous enclosure saturated with a Cu–water nanofluid. *J. Therm. Anal. Calorim.* **2017**, *29*, 052001. [[CrossRef](#)]
31. Alsabery, A.I.; Ismael, M.A.; Chamkha, A.J.; Hashim, I. Effects of two-phase nanofluid model on MHD mixed convection in a lid-driven cavity in the presence of conductive inner block and corner heater. *J. Therm. Anal. Calorim.* **2018**, 1–22. [[CrossRef](#)]
32. Maxwell, J.C. *A Treatise on Electricity and Magnetism, Vol. II. Clarendon*; Oxford University Press: Oxford, UK, 1904.
33. Corcione, M. Empirical correlating equations for predicting the effective thermal conductivity and dynamic viscosity of nanofluids. *Energy Convers. Manag.* **2011**, *52*, 789–793. [[CrossRef](#)]
34. Alsabery, A.; Tayebi, T.; Chamkha, A.; Hashim, I. Effect of rotating solid cylinder on entropy generation and convective heat transfer in a wavy porous cavity heated from below. *Int. Commun. Heat Mass Transf.* **2018**, *95*, 197–209. [[CrossRef](#)]
35. Calcagni, B.; Marsili, F.; Paroncini, M. Natural convective heat transfer in square enclosures heated from below. *Appl. Therm. Eng.* **2005**, *25*, 2522–2531. [[CrossRef](#)]
36. Ho, C.J.; Liu, W.K.; Chang, Y.S.; Lin, C.C. Natural convection heat transfer of alumina-water nanofluid in vertical square enclosures: An experimental study. *Int. J. Therm. Sci.* **2010**, *49*, 1345–1353. [[CrossRef](#)]
37. Sheikhzadeh, G.A.; Dastmalchi, M.; Khorasanizadeh, H. Effects of nanoparticles transport mechanisms on Al₂O₃-water nanofluid natural convection in a square enclosure. *Int. J. Therm. Sci.* **2013**, *66*, 51–62. [[CrossRef](#)]
38. Motlagh, S.Y.; Soltanipour, H. Natural convection of Al₂O₃-water nanofluid in an inclined cavity using Buongiorno's two-phase model. *Int. J. Therm. Sci.* **2017**, *111*, 310–320. [[CrossRef](#)]
39. Corcione, M.; Cianfrini, M.; Quintino, A. Two-phase mixture modeling of natural convection of nanofluids with temperature-dependent properties. *Int. J. Therm. Sci.* **2013**, *71*, 182–195. [[CrossRef](#)]
40. Chon, C.H.; Kihm, K.D.; Lee, S.P.; Choi, S.U. Empirical correlation finding the role of temperature and particle size for nanofluid (Al₂O₃) thermal conductivity enhancement. *Appl. Phys. Lett.* **2005**, *87*, 3107. [[CrossRef](#)]
41. Bergman, T.L.; Incropera, F.P. *Introduction to Heat Transfer*, 6th ed.; Wiley: New York, NY, USA, 2011.

